ORIGINAL PAPER

Journal of Textile Engineering (2007), Vol.53, No.1, 9 - 15

Numerical Analysis of Penetration Flow through Viscoelastic Fluids

YAMAMOTO Takehiro*, KIMOTO Ryusuke

Department of Mechanical Engineering, Graduate School of Engineering, Osaka University, 2-1 Yamadaoka, Suita, Osaka 565–0871, Japan

Received 8 September 2006; accepted for publication 10 January 2007

Abstract

Penetration flows of a Newtonian fluid through a viscoelastic fluid in an abrupt contraction channel were numerically analyzed. In the numerical simulation, the Phan-Thien Tanner model was employed as a constitutive equation. The level set method was used to numerically represent the interface between two fluids and effects of interfacial tension were introduced into the numerical simulation using the continuum surface force model. The numerical computation predicted the occurrence of fluctuation of interface between a Newtonian penetrating fluid and a viscoelastic fluid in a downstream conduit of the contraction channel. This fluctuation was a typical phenomenon for penetration flows through a viscoelastic fluid and was not observed in a penetrate flow through a Newtonian fluid. Furthermore, it was confirmed that the normal stress effect drove the fluctuation and the amplitude of fluctuation when elastic properties were strong.

Key Words: Penetration flow, Viscoelastic fluid, Interface, Numerical simulation, Phan-Thien Tanner model

1. Introduction

We often encounter penetration flows of a fluid through another one in industrial processes such as a sandwich injection molding, a lamellar injection molding, and manufacturing process of hollow fibers. In penetration flows, an interface between two fluids shows various phenomena depending on flow conditions. For example, when a less viscous fluid is injected into a more viscous fluid, the interface of two fluids is fundamentally unstable and grows to form a complicated pattern, which is called viscous fingers. This phenomenon relates many problems in physics, chemistry, engineering, and so on and has been studied by many researchers [1–3]. The authors also studied viscous fingering in polymer solutions [4–6] and surfactant solutions [7]. The behavior of interface is an important issue in industry because it affects the quality and function of final products. In addition, polymer solutions and melts are utilized in many products and viscoelastic flow behavior of these fluids is very complicated. Consequently, it is useful to investigate the interface behavior in viscoelastic fluids and obtain its knowledge.

In the present study, we considered penetration flows of a Newtonian fluid through a Newtonian or a viscoelastic fluid and performed numerical simulation of the flow in a contraction channel to analyze the effects of viscoelasticity on the behavior of interface. The finite volume method (FVM) was applied to solve basic equations. In addition, the interface was numerically expressed with the level set method [8], and a CIP method [9] is used to solve an advection equation that describes the movement of interface. Moreover, the Phan-Thien Tanner (PTT) model [10, 11] was employed as a constitutive equation. This model has been successfully used in many numerical simulations of viscoelastic flows such as pipe flow [12], contraction flows [13, 14], flows in dies [15], melt spinning of hollow fibers [16], three-dimensional flows through a channel with a cavity [17], and dip coating flows [18].

2. Basic equations

Basic equations include the equation of continuity, the equation of motion, and a constitutive equation. The equation of continuity (1) and the equation of motion (2) denoted using Einstein's summation rule are as follows:

$$\frac{\partial u_i}{\partial x_i} = 0 , \tag{1}$$

$$\frac{\partial (\rho u_i)}{\partial t} + \frac{\partial}{\partial x_k}(\rho u_i u_k) = \frac{\partial \sigma_{ik}}{\partial x_k} + F_i , \tag{2}$$

where ρ is the density, t is time, u_i is the x_i-component of velocity vector, and σ_{ik} is the ik-component of the total

Corresponding author: E-mail: take@mech.eng.osaka-u.ac.jp, Tel: +81-6-6879-7308, Fax: +81-6-6879-7308

stress tensor. F_i is the x_i-component of external force vector. It should be noted that Einstein's summation rule is also applied to denote other equations in the present paper. The stress tensor is divided into the isotropic pressure component $-p\delta_{ij}$ and the extra stress tensor S_{ij} as follows:

$$\sigma_{ij} = -p\delta_{ij} + S_{ij}, \tag{3}$$

where p is the pressure, δ_{ij} is Kronecker's delta. It can be assumed that S_{ij} is divided into a Newtonian contribution $2\eta_N d_{ij}$ and a polymer contribution τ_{ij} as $S_{ij} = 2\eta_N + \tau_{ij}$, where d_{ij} is the rate-of-deformation tensor defined by $d_{ij} = (\partial u_i/\partial x_j + \partial u_j/\partial x_i)/2$.

The Phan-Thien Tanner model [10, 11] is employed as a constitutive equation. In this model, the polymer contribution to the stress tensor τ_{ij} obeys the following equations:

$$g\tau_{ij} + \lambda \frac{\delta \tau_{ij}}{\delta t} = 2\eta_p d_{ij}, \tag{4}$$

$$g = 1 + \frac{\lambda\varepsilon}{\eta_p}\tau_{ij}, \tag{5}$$

where the differential operator $\delta/\delta t$ means the upper-convective time derivative for the simplified PTT model [10, 11]. ε is a parameter with a value between zero and unity.

In the present computation, we employed the elastic-viscous split-stress (EVSS) method [14, 19, 20] to stabilize the numerical scheme. In the EVSS method, the stress tensor S_{ij} is describe by

$$S_{ij} = 2\eta_0 d_{ij} + T_{ij}, \tag{6}$$

$$T_{ij} = \tau_{ij} - 2\beta\eta_0 d_{ij}, \tag{7}$$

where T_{ij} is called the elastic stress tensor and β is defined by $\beta = \eta_p/\eta_0 = \eta_p/(\eta_p + \eta_N)$. Substituting Eqs (3), (6), and (7) into Eqs (2) and (4), one obtains the following equations:

$$\frac{\partial(\rho u_i)}{\partial t} + \frac{\partial}{\partial x_k}(\rho u_k u_i) - \eta_0 \frac{\partial}{\partial x_k}\left(\frac{\partial u_i}{\partial x_k}\right) = -\frac{\partial p}{\partial x_i} + \frac{\partial T_{ik}}{\partial x_k} + F_i, \tag{8}$$

$$gT_{ij} + \lambda \frac{\delta T_{ij}}{\delta t} = 2\beta\eta_0 \left[(1-g)\, d_{ij} - \lambda \frac{\delta}{\delta t} d_{ij}\right]. \tag{9}$$

Numerical computations were performed based on a non-dimensionalized basic equations. Physical quantities were scaled as $t^* = t/(H/U)$, $x_i^* = x_i/H$, $u_i^* = u_i/U$, $p^* = p/(\eta_0 U/H)$, $T_{ij}^* = T_{ij}/(\eta_0 U/H)$, $d_{ij}^* = d_{ij}/(U/H)$, and $F_i^* = F_i/(\eta_0 U/H)$, where symbols with asterisk (*) indicate non-dimensional variables and H and U are the representative length and velocity, respectively. Consequently, one obtains the following equations in a non-dimensional form:

$$\frac{\partial u_i^*}{\partial x_i^*} = 0, \tag{10}$$

$$\frac{\partial u_i^*}{\partial t^*} + \frac{\partial}{\partial x_k^*}(u_k^* u_i^*) = \frac{1}{Re}\left(-\frac{\partial p^*}{\partial x_i^*} + \frac{\partial^2 u_i^*}{\partial x_k^{*2}} + \frac{\partial T_{ik}^*}{\partial x_k^*} F_i^*\right), \tag{11}$$

$$\frac{\partial T_{ij}^*}{\partial t^*} + u_k^* \frac{\partial T_{ij}^*}{\partial x_k^*} = 2\beta_0 \left[\frac{(1-g)}{We} d_{ij}^* - \left\{\frac{\partial d_{ij}^*}{\partial t^*} + \frac{\partial}{\partial x_k^*}(u_k^* d_{ij}^*) - \frac{\partial u_i^*}{\partial x_k^*} d_{kj}^* - \frac{\partial u_j^*}{\partial x_k^*} d_{ki}^*\right\}\right] - \frac{g}{We} T_{ij}^* + \frac{\partial u_i^*}{\partial x_k^*} T_{kj}^* + \frac{\partial u_j^*}{\partial x_k^*} T_{ki}^*. \tag{12}$$

The Reynolds number Re and the Weissenberg number We are defined by $Re = \rho UH/\eta_0$ and $We = \lambda U/H$, respectively.

3. Numerical scheme

3.1 Problem setting and numerical method

We consider penetrating flows in a two-dimensional abrupt contraction channel in Fig.1. The contraction ratio of the channel is 2 to 1 and the half height of a narrow channel is H, which is the representative length. The flow direction is x and the y axis is perpendicular to the flow direction. The mean velocity in the downstream channel is chosen as the representative velocity U. Two types of flows are numerically simulated: one is a flow of a Newtonian fluid penetrating through another Newtonian fluid and the other is a Newtonian fluid flow penetrating through a viscoelastic fluid. The former is denoted by N/N case, and the latter is done by N/VE case in the present paper. The initial interface is flat and locates at $x = -4.8H$ perpendicular to the x-axis shown in Fig. 1. The no-slip condition is adopted on the channel wall and fully developed flow conditions are adopted at both the inlet and outlet of the channel. Although the dynamic contact angle should be given at the contact points of two fluids and the wall for precise simulation of interface behavior near the contact point, it is not given in the present computation because it is not easy to choose proper values of the contact angle and the flow behavior near the contact points may not significantly affect the interface behavior in the downstream channel, which we focus in the present analysis.

PTT fluids have typical viscoelastic properties. Rheological properties of PTT fluids such as the non-

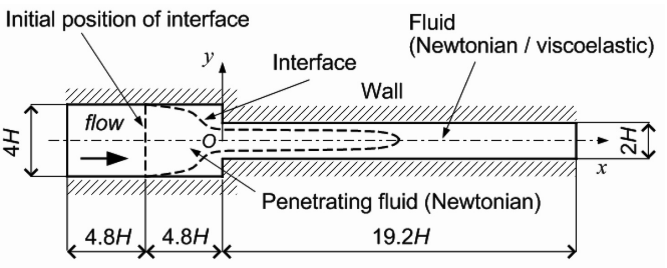

Fig. 1 Schematic diagram of abrupt contraction channel and problem considered.

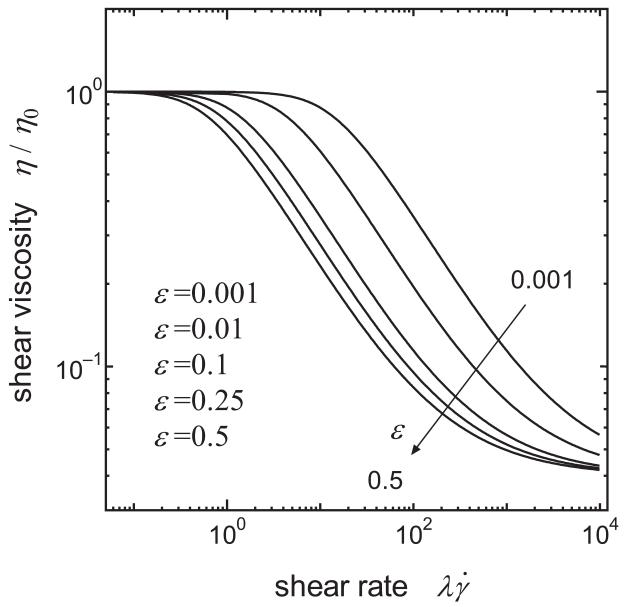

Fig. 2 Non-dimensional shear viscosity η/η_0 as a function of non-dimensional shear rate $\lambda\dot{\gamma}$.

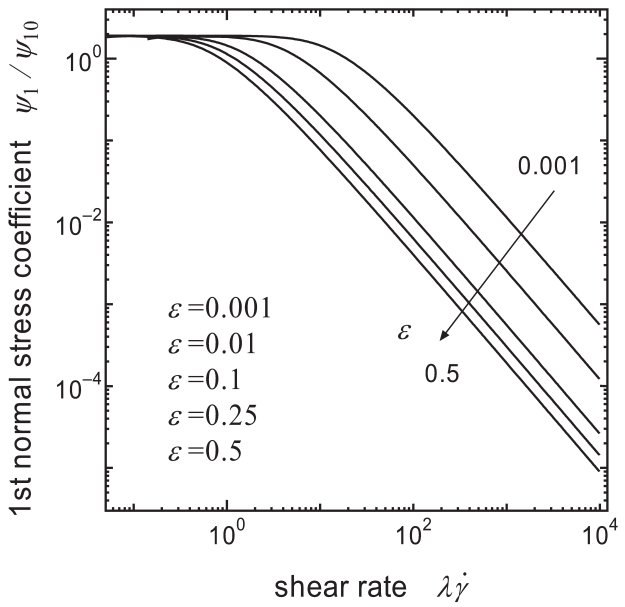

Fig. 3 Non-dimensional first normal stress coefficient $\psi_1/\psi_{10}=N_1/(\eta_0\lambda\dot{\gamma}^2)$ as a function of non-dimensional shear rate $\lambda\dot{\gamma}$.

dimensional shear viscosity η/η_0 and the non-dimensional first normal stress coefficient $\psi_1/\psi_{10}=N_1/(\eta_0\lambda\dot{\gamma}^2)$ are shown in Figs. 2 and 3, respectively. In the present simulation, the viscosity ratio η_s/η_0 is 0.04. PTT fluids show shear-thinning properties in both η and ψ_1. The value of ψ_1 is large at small ε and hence elastic properties are stronger for smaller ε. In addition, PTT fluids have stretch-thickening elongation viscosity. Their elongation viscosities show stronger strain-thickening property for smaller ε and grow faster for larger ε [17, 18].

The basic equations are discretized with a FVM, and a hybrid scheme [21, 22] is used to stabilize the numerical scheme. In addition, SIMPLE scheme is adopted for a coupling method of the equation of motion and the equation of continuity. The detail of SIMPLE scheme is available in several literatures (e.g. [21, 22, 23]).

3. 2 Expression of interface

In the present problem, we should numerically express the interface between two fluids. We employed the level set method [8, 24], in which, a signed distance function from an interface f is considered and the interface is expressed by a contour of $f = 0$. A region of $-\alpha \le f \le \alpha$ is treated as a transition zone between two fluids. In this region, an approximate Heaviside function $H_\alpha(f)$ defined by

$$H_\alpha(f) = \begin{cases} -0.5 & (f > \alpha) \\ 0.5\left(\frac{f}{\alpha} + \frac{1}{\pi}\sin\left(\frac{\pi f}{\alpha}\right)\right) & (|f| \le \alpha) \\ 0.5 & (f > -\alpha) \end{cases} \quad (13)$$

is used to interpolate density ρ and viscosity η in N/N case as

$$\rho(f) = 0.5\,(\rho_1+\rho_2) + (\rho_1-\rho_2)H_\alpha(f)\,, \quad (14)$$

$$\eta(f) = 0.5\,(\eta_1+\eta_2) + (\eta_1-\eta_2)H_\alpha(f)\,, \quad (15)$$

where the subscripts 1 and 2 specify a fluid. In N/VE case, density and the extra stress is interpolated in a similar way of N/N case.

The movement of interface is computed based on the advection equation of f:

$$\frac{\partial f}{\partial t} + v_i \frac{\partial f}{\partial x_i} = 0\,. \quad (16)$$

The distance function f has a property that $|\nabla f|=1$. This property, however, diminishes during the numerical computation. Hence, the property is restored with a re-initialization procedure, which is denoted by the following equations:

$$\frac{\partial f}{\partial \tilde{t}} + S(f)\,(1-|\nabla f|) = 0\,, \quad (17)$$

$$S(f) = \frac{f}{\sqrt{f^2+\delta^2}}(1-|\nabla f|) = 0\,, \quad (18)$$

where $\tilde{t}$ is time for progressing the re-initialization process and is not necessarily equal to t. δ is a value with the dimension of length and is usually chosen as 1.5 to 3.5 times of the representative size of computational cell. In the present computation, δ is 1.5 times of the cell size. Furthermore, we adopted a volume conserving re-initialization method proposed by Chang et al. [24] to conserve the volume of a penetrating fluid. Equations (16),

(17), and (18) are non-dimensionalized in a manner similar to the non-dimensionalization method for the basic equations and are numerically solved with a CIP method [9].

The effect of interfacial tension is introduced into the computation using the continuum surface force (CSF) model [25]. In this model, the surface force due to the interfacial tension is translated to an equivalent volume force $\boldsymbol{F}_v$ defined by

$$\boldsymbol{F}_v = -\gamma \left\{ \nabla \cdot \left(\frac{\nabla f}{|\nabla f|} \right) \right\} \cdot \nabla H_\alpha \,, \tag{19}$$

where γ is the surface tension. $\boldsymbol{F}_v$ is included in the external force term in Eq (11). Consequently Eq (11) becomes

$$\frac{\partial u_i^*}{\partial t^*} + \frac{\partial}{\partial x_k^*}(u_k^* u_i^*) = -\frac{1}{Re}\left(\frac{\partial p^*}{\partial x_i^*} + \frac{\partial^2 u_i^*}{\partial x_k^{*2}} + \frac{\partial T_{ik}^*}{\partial x_k^*} + \frac{1}{Ca}(F_v)_i^* \right) \tag{20}$$

where Ca is the capillary number defined by $Ca = \eta_0 U/\gamma$.

4. Results

4. 1 N/N case

Firstly, we consider N/N case. The ratio of dynamic viscosity is kept to 1 and the capillary number and the Reynolds number are varied. Figure 4 shows the evolution of interface between two Newtonian fluids at Re=10 and Ca=1.2. One fluid (gray) penetrates into the other fluid (black). A protrusion part passes through the contraction and flows into the downstream channel. The width of protrusion in the downstream channel varies with position: The width of protrusion decreases with increasing x, shows an inflection point, and slightly increases to reach a steady state value in a downstream region.

We evaluate the replacement ratio r_R defined by the ratio of protrusion width to the channel width to investigate the dependence of the width on Ca and Re. Figure 5 shows change in r_R with time t^* at x = 9.6H, where t^* means dimensionless elapsed time from the startup of flow. When the protrusion reaches this position, r_R quickly increases, fluctuates because of passage of a constriction part of protrusion, and gradually approaches a steady value. At large capillary numbers, this phenomenon is clearly observed, while at small capillary numbers the fluctuation is not seen because constriction part is little. The width of protrusion is wider, i.e. r_R is larger, for smaller Ca. Figure 6 shows the dependence of r_R on Ca in a far downstream region where the width of protrusion is nearly constant. The value of r_R approaches around 0.5 with increasing Ca. This result is consistent with a two-dimensional numerical simulation for a straight channel [26] and experimental results of viscous fingering in a Hele-Shaw cell [27]. We

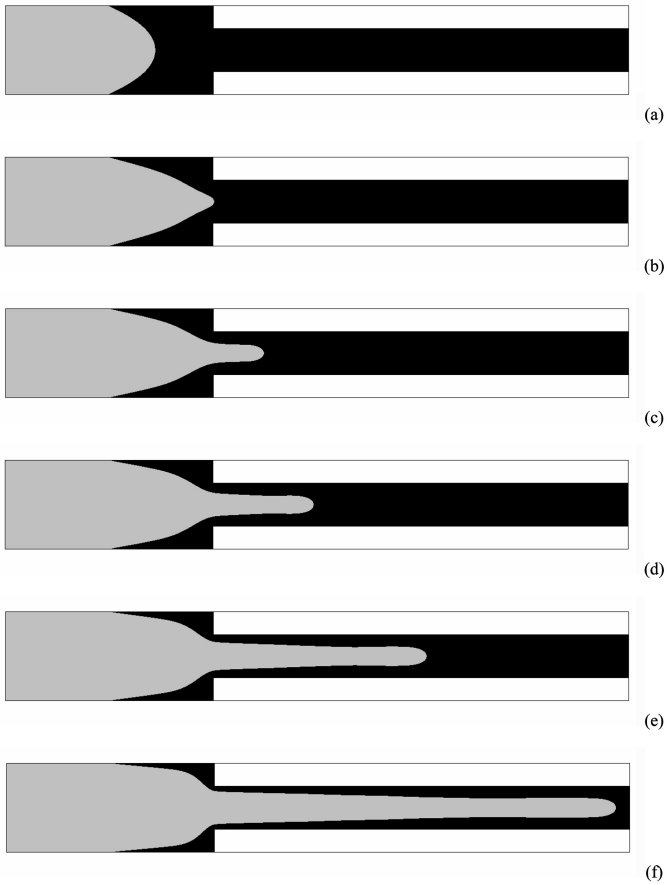

Fig. 4 Evolution of interface between a penetrating Newtonian fluid (gray) and a Newtonian fluid (black) at Re=10 and Ca=1.2: (a) t^*=3.1, (b) t^*=6.2, (c) t^*=7.8, (d) t^*=9.4, (e) t^*=12.9, and (f) t^*=18.7.

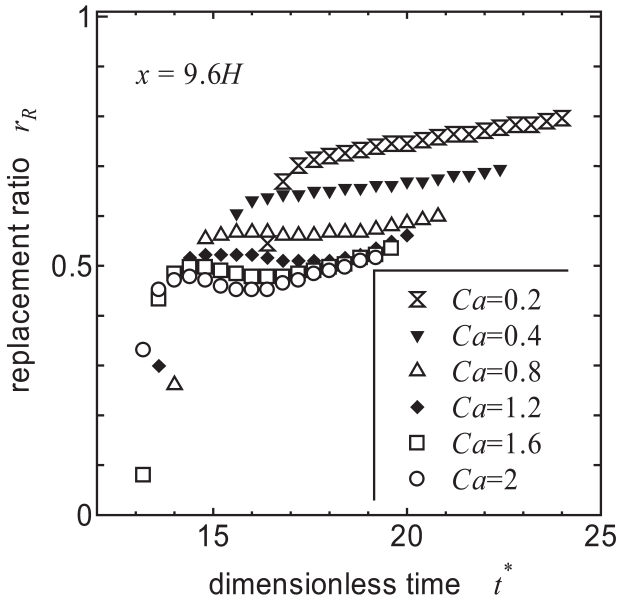

Fig. 5 Change in replacement ratio r_R with time t^* at x=9.6H for Re = 10 and Ca = 0.2, 0.4, 0.8, 1.2, 1.6, and 2.

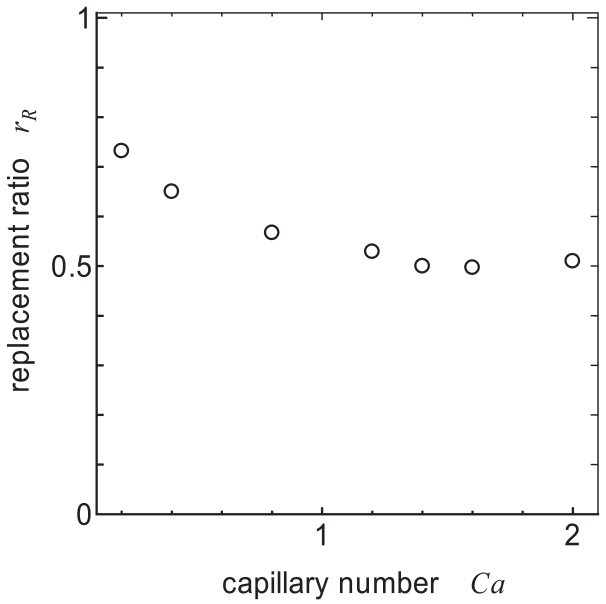

Fig. 6 Dependence of replacement ratio r_R on the capillary number Ca in a far downstream region where the width of protrusion is nearly constant.

also performed calculations by changing Re in a range of 2.5 to 10. However, significant difference is not seen among the results of each Re. Hence Ca is dominant in the range of Re between 2.5 and 10 for the interface behavior.

4. 2 N/VE case

Here we investigate the penetration flow through a viscoelastic fluid. The ratio of dynamic viscosity of a Newtonian fluid to that of a viscoelastic fluid is kept to 0.01, where the dynamic viscosity of viscoelastic fluid is evaluated by the zero-shear-rate viscosity divided by density. Figure 7 shows the evolution of interface between a penetrating Newtonian fluid (gray) and a viscoelastic fluid (black) at Re=10, Ca=2, We=0.5, and ε=0.001. The protrusion shows similar behavior to the counterpart of N/N case at early stages. However, a fluctuation of interface, which is not observed in N/N case, appears as the protrusion progresses (Fig. 7e, 7f).We focus this phenomenon and investigate its mechanism. Figure 8 shows shapes of interface when protrusions progresses enough. The results at Re=10, Ca=2, ε=0.001, and We=0.2, 0.4, and 0.6 are indicated. The fluctuation of interface is not seen clearly at We=0.2, and appears remarkably at large We. Especially at We=0.6, the shape of interface is drastically changed by the fluctuation. These results indicate that elastic properties of viscoelastic fluid strongly affect the fluctuation. In addition, results of computations for various values of ε, which are discussed later, show that the amplitude of fluctuation is larger for smaller ε. These results suggest that the

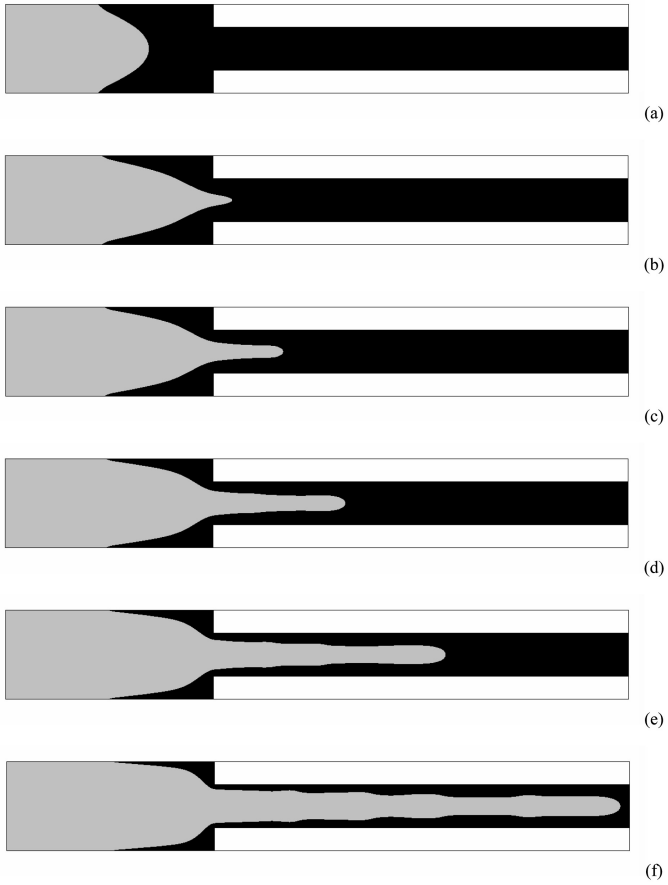

Fig. 7 Evolution of interface between a penetrating Newtonian fluid (gray) and a viscoelastic fluid (black) at Re=10, Ca=2, We=0.5, and ε=0.001: (a) t^*=3.1, (b) t^*=6.6, (c) t^*=8.2, (d) t^*=9.8, (e) t^*=12.9, and (f) t^*=19.1.

fluctuation appears strongly under highly elastic conditions.

Figure 9 shows the change in r_R with time for Re=10, Ca= 2, We=0.5, and ε=0.001, 0.01, 0.1, 0.25, and 0.5 at x=4.8H and 9.6H. At both positions, we can see the fluctuation in r_R with time, which is not observed in N/N case. Values of r_R increase with fluctuating and approach to steady state values and the cycle of fluctuation is similar in both cases. At x=4.8H, effects of ε are weak and significant difference among the results is not seen. On the other hand, at x=9.6H, comparison of distance between a peak and a trough after t^* around 10 indicates that small difference appears and the distance is larger for smaller ε, i.e. for more elastic fluids. Consequently the fluctuation appears more strongly under more elastic condition. The fluctuation is not observed just downstream of the entrance to the contraction and appears in a wide region downstream of the contraction. This means that a fluctuation of interface emerges owing to a flow behavior near the contraction and some mechanism for driving the fluctuation exists. In addition, numerical predictions suggest that elastic properties of viscoelastic fluid relate the fluctuation. Consequently, we will next investigate the mechanism of fluctuation by analyzing the

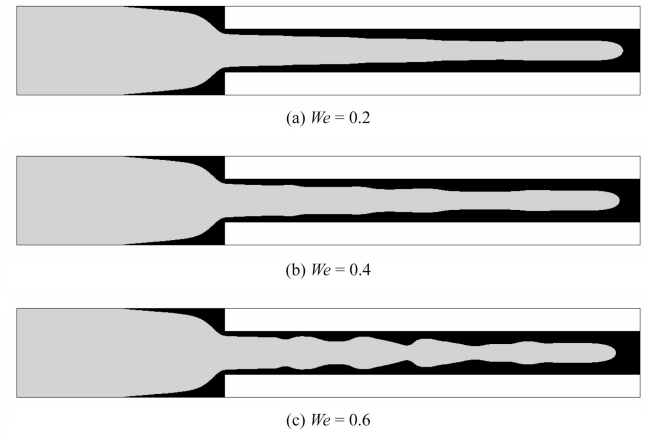

Fig. 8 Interface between a penetrating Newtonian fluid (gray) and a viscoelastic fluid (black) when protrusions progresses enough at Re=10, Ca=2, and ε=0.001: We=(a) 0.2, (b) 0.4, and (c) 0.6.

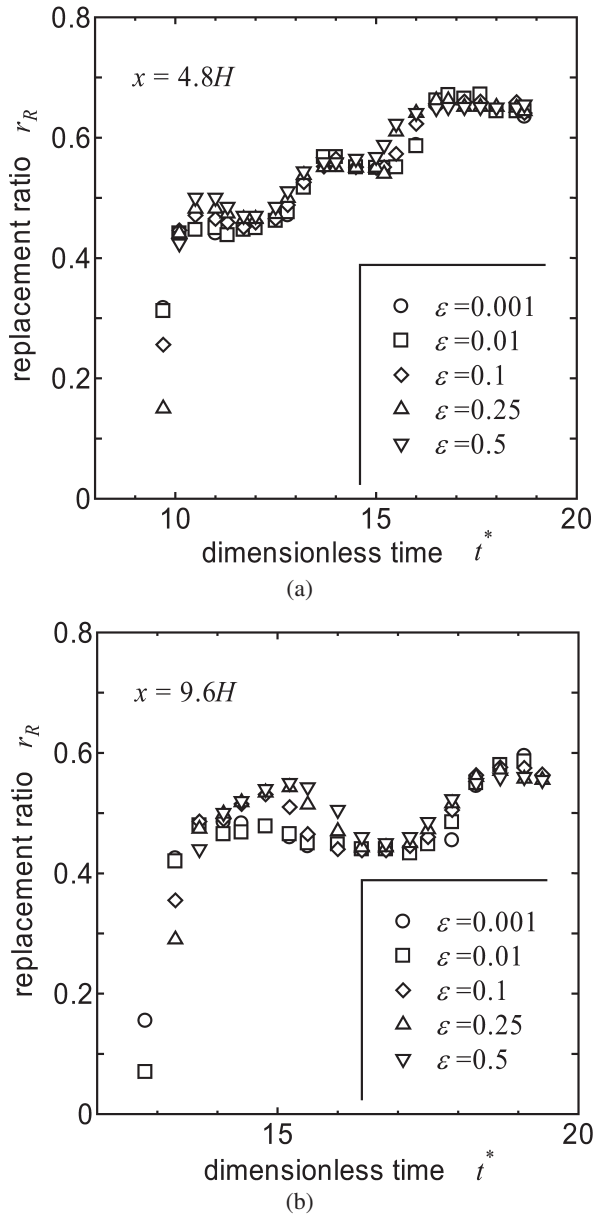

Fig. 9 Change in the replacement ratio r_R with dimensionless time t^* at x=4.8H and 9.6H for Re=10, Ca=2, and We= 0.5.

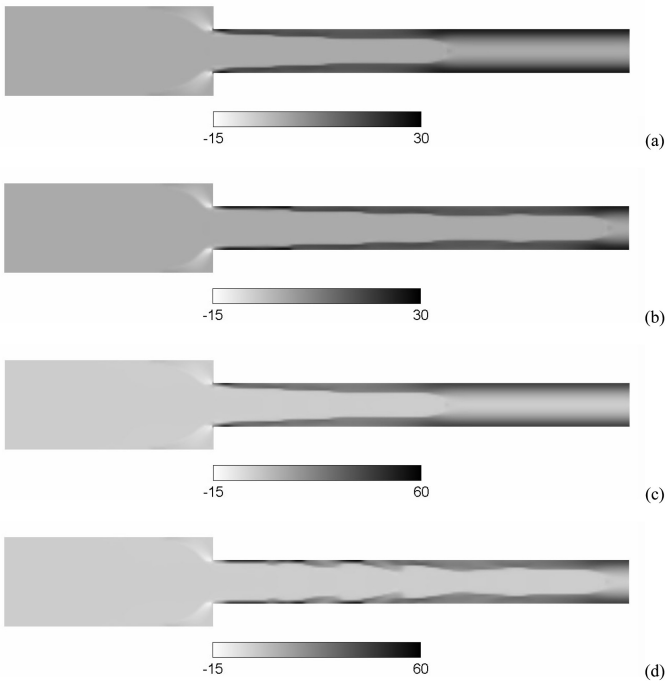

Fig. 10 Distribution of normal stress difference $\tau_{xx}-\tau_{yy}$ at Re=10, Ca=2, and ε=0.001: (a) We=0.5, t^*=12.9, (b) We= 0.5, t^*=19.1, (c) We=0.6, t^*=12.9, and (d) We=0.6, t^*= 19.1.

numerical results of stress field to clarify the mechanism.

We analyze the stress field to confirm the relation between the interface fluctuation and the fluid elasticity. Fig. 10 shows the distribution of normal stress difference $\tau_{xx}-\tau_{yy}$ at Re = 10, Ca = 2, We = 0.5 and 0.6. In Fig. 10, $\tau_{xx}-\tau_{yy}$ in the downstream channel distributes parallel to the channel wall and is large near the wall when a protrusion does not penetrate the channel enough and after the protrusion flows into the downstream channel more, regions of large $\tau_{xx}-\tau_{yy}$ appear. When a fluctuation of interface begins, the stress distribution changes and $\tau_{xx}-\tau_{yy}$ increases in a narrow viscoelastic film region, where the force towards the channel center is large. This phenomenon appears remarkably at larger We, i.e. We=0.6. On the other hand, in a wide viscoelastic film, $\tau_{xx}-\tau_{yy}$ is small. In large normal stress difference regions, the viscoelastic fluid pushes the Newtonian protrusion inside the channel and the protrusion narrows. These elastic effects have been observed also in gas penetration flows through a viscoelastic fluid in a tube [28]. The narrowed protrusion tends to spread until its width reaches that when the normal force effect does not exist, i.e. the width of a corresponding N/N case, and hence the fluctuation continues. The position of a large $\tau_{xx}-\tau_{yy}$ region moves little with time after the region appears. At higher Weissenberg numbers, the stress difference is larger and hence the fluctuation appears more strongly. In the present flow problem, elongational properties of viscoelastic fluid are not very important because a viscoelastic fluid does not

exists in a region where elongational flow is dominant, and the shear flow near the channel wall in flows in the downstream channel strongly affects this fluctuation flow phenomenon.

The magnitude of $\tau_{xx}-\tau_{yy}$ is relatively large near the reentrance corner of contraction and this stress distribution is a trigger of the fluctuation. In addition, just downstream of the contraction, the velocity vector has a component towards the channel center and hence velocity component in the $y-$direction turns its sign just downstream of the contraction for approaching a steady velocity distribution whose $y-$component is zero. This development in velocity distribution is also a possibility of a trigger of the fluctuation. Once a fluctuation occurs, it is driven by the normal force effect in N/VE cases.

5. Conclusion

We numerically analyzed penetration flows through a viscoelastic fluid in an abrupt contraction channel with the PTT model as a constitutive equation and with the level set method as a numerical expression of interface between two fluids. The numerical computation indicates that the fluctuation of interface between a Newtonian penetrating fluid and a viscoelastic fluid occurs in the downstream conduit of the contraction channel. This fluctuation is a typical phenomenon for penetration flows through a viscoelastic fluid and is not observed in a penetrate flow through a Newtonian fluid. Furthermore, numerical simulations predict that the elastic property, i.e. the normal stress effect, drives the fluctuation. If the Weissenberg number is much higher, interface instabilities following an interface fluctuation will occur, which are interesting and important problems in a practical point of view. However, some improvements in numerical scheme are necessary for the simulation at high Weissenberg numbers.

References

[1] Homsy GM (1987) Annu Rev Fluid Mech, **19**, 271–311

[2] Vicsek T (1989) "Fractal Growth Phenomena", Chap 10, World Scientific Publishing, Singapore

[3] Tanveer S (2000) J Fluid Mech, **409**, 273–308

[4] Yamamoto T, Kamikawa H, Tanaka H, Nakamura K, Mori N (2001) Nihon Reoroji Gakkaishi, **29**, 81–87

[5] Yamamoto T, Kamikawa H, Mori N, Nakamura K (2002) Nihon Reoroji Gakkaishi, **30**, 121–127

[6] Yamamoto T, Kimoto R, Mori N (2005) JSME Int J, Ser B, **48**, 756–762

[7] Yamamoto T, Nakamura Y, Yamashita A, Hashimoto T, Mori N (2006) Rheol Acta, **45**, 250–259

[8] Sussman M, Smereka P, Osher S (1994) J Comput Phys, **114**, 146–159

[9] Yabe T, Utsumi T, Ogata Y (2003) "CIP method", Morikita Publishing, Tokyo

[10] Phan-Thien N, Tanner RI (1977) J Non-Newtonian Fluid Mech, **2**, 353–365

[11] Phan-Thien N (1978) J Rheol, **22**, 259–283

[12] Pinho FT, Oliviera PJ (2000) Int J Heat Mass Trans, **43**, 2273–2287

[13] Azaiez J, Guenette R, Ait-Kadi A (1996) J Non-Newtonian Fluid Mech, **62**, 253–277

[14] Xue SC, Phan-Thien N, Tanner RI (1998) J Non-Newtonian Fluid Mech, **74**, 195–245

[15] Kihara S, Gouda T, Matsunaga K, Funatsu K (1999) Polym Eng Sci, **39**, 152–163

[16] de Rovere A, Shambaugh RL (2001) Polym Eng Sci, **41**, 1206–1219

[17] Yamamoto T, Ishiyama M, Nakajima M, Nakamura K, Mori N (2003) J Non-Newtonian Fluid Mech, **114**, 13–31

[18] Yamamoto T, Nojima N, Mori N (2005) J Text Eng, **51**, 21–28

[19] Baaijens FPT (1998) J Non-Newtonian Fluid Mech, **79**, 361–385

[20] Owens RG, Phillips TN (2002) "Computational Rheology", Imperial College Press, London

[21] Patankar SV (1980) "Numerical Heat Transfer and Fluid Flow", Hemisphere Publishing, New York

[22] Arakawa C (1994) "Computational Fluid Dynamics for Engineering", Univ of Tokyo Press, Tokyo

[23] Ferziger JH, Perić M (1996) "Computational Methods for Fluid Dynamics", Springer-Verlag, Berlin

[24] Chang YC, Hou TY, Merriman B, Osher S (1996) J Comput Phys, **124**, 449–464

[25] Brackbill JU, Kothe DB, Zemach C (1992) J Comput Phys, **100**, 335–354

[26] Kamisli F, Ryan ME (2002) Int J Numer Meth Fluids, **38**, 407–427

[27] Lindner A, Bonn D, Meunier J (2000) Phys Fluids, **12**, 256–261

[28] Yamamoto T, Suga T, Nakamura K, Mori N (2004) J Fluids Eng, **126**, 148–152